Microsc. Microanal. 10, 146–152, 2004
DOI: 10.1017/S1431927604040358

Microscopy AND Microanalysis



# Observation of Magnetic Multilayers by Electron Holography

T. Tanji,[1]* S. Hasebe,[1] Y. Nakagami,[1] K. Yamamoto,[2] and M. Ichihashi[3]

[1]*Department of Electronics, Nagoya University, Nagoya 464-8603, Japan*
[2]*Japan Science and Technology Corporation, c/o Japan Fine Ceramics Center, Nagoya 465-8587, Japan*
[3]*Center for Integrated Research in Science and Engineering, Nagoya University, Nagoya 464-8603, Japan*

**Abstract:** Magnetic structures of Co/Cu multilayers in cross section are observed by two kinds of electron holography: a Fourier method and a phase-shifting method, which is introduced briefly. The Fourier method can easily reconstruct wave functions and is applied to many specimens, whereas the phase-shifting method requires longer time for processing, but has a higher spatial resolution that permits us to discuss fine structures. Magnetization vectors in Co layers aligning parallel and separating into two blocks with antiparallel alignment are observed. Magnetic blurring on the boundary between Co and Cu in the reconstructed phase images is larger than the estimated atomic roughness.

**Key words:** multilayer, electron holography, phase-shifting method, Co/Cu

## Introduction

Magnetic materials are subjected to many types of investigations, which include observations of magnetic structures. Today's advanced information-oriented society requires very high density recording media, which in turn demands materials of high fineness. Therefore, observation of micromagnetic structures is eagerly desired, to enable evaluation of such structures. Magnetic multilayers, in which ferromagnetic layers measuring a few nanometers in thickness are alternately stacked with para- or antiferromagnetic layers, are new artificial materials attracting a great deal of attention. Giant magnetoresistance (GMR) of magnetic multilayers (Baibich et al., 1988) is the effect whereby electric resistance is drastically reduced in an external magnetic field, and is expected to find application in a new magnetic sensor. Some multilayers, such as spin valve films, have already been applied to a magnetic head.

The origin of GMR is considered to be as follows: Magnetization vectors in ferromagnetic layers separated by spacer layers of proper thickness align antiparallel to those in adjacent ferromagnetic layers in response to exchange coupling in a magnetic-free space, where both electrons with up- and down-spin moment are scattered at the boundaries, resulting in high electric resistance. In contrast, realignment of magnetization vectors to be parallel in a suitable external magnetic field causes scattering of only one kind of electron, with either up- or down-spin, and lowers such spin-dependent electric resistance. The intensity of the exchange coupling, which corresponds to the amplitude of GMR, depends on the thickness of spacer layers. As the thickness of spacer layers is increased, the ratio of magnetoresistance decreases and shows oscillative behavior (Parkin et al., 1990; Dorner et al., 1993). We have observed magnetic structures of multilayers by Lorentz microscopy and electron holography (Tanji et al., 2002).

In the present investigation, the structures of Co/Cu multilayered films are observed in cross section by electron holography using a transmission electron microscope (TEM).

Received January 9, 2003; accepted June 13, 2003.
*Corresponding author. E-mail: tanji@nuee.nagoya-u.ac.jp

## Materials and Methods

### Specimen

Multilayers Co(4.0 nm)/Cu($x$ nm), $x$ = 1.5, 2.0, 2.5, and 3.5 have been prepared by RF-magnetron sputtering on Si substrates at room temperature. The background pressure is $7 \times 10^{-5}$ Pa, and the partial pressure of Ar is $3 \times 10^{-1}$ Pa. Figure 1 shows magnetization characteristics of Si/$[\mathrm{Co}(4.0\ \mathrm{nm})/\mathrm{Cu}(x\ \mathrm{nm})]_4$ multilayers as measured by an alternating gradient magnetometer (AGM); the sample of $x$ = 2.0 nm seems to have the strongest antiferromagnetic alignment, whose ratio of saturation magnetization to residual magnetization (Ms/Mr), 0.18, and coercive force (Hc), 10.1 Oe, are the smallest among the four samples. This sample roughly corresponds to the second maximum of Co/Cu magnetoresistance ratio, $\Delta R/R_0$ ($\Delta R$: decrease of

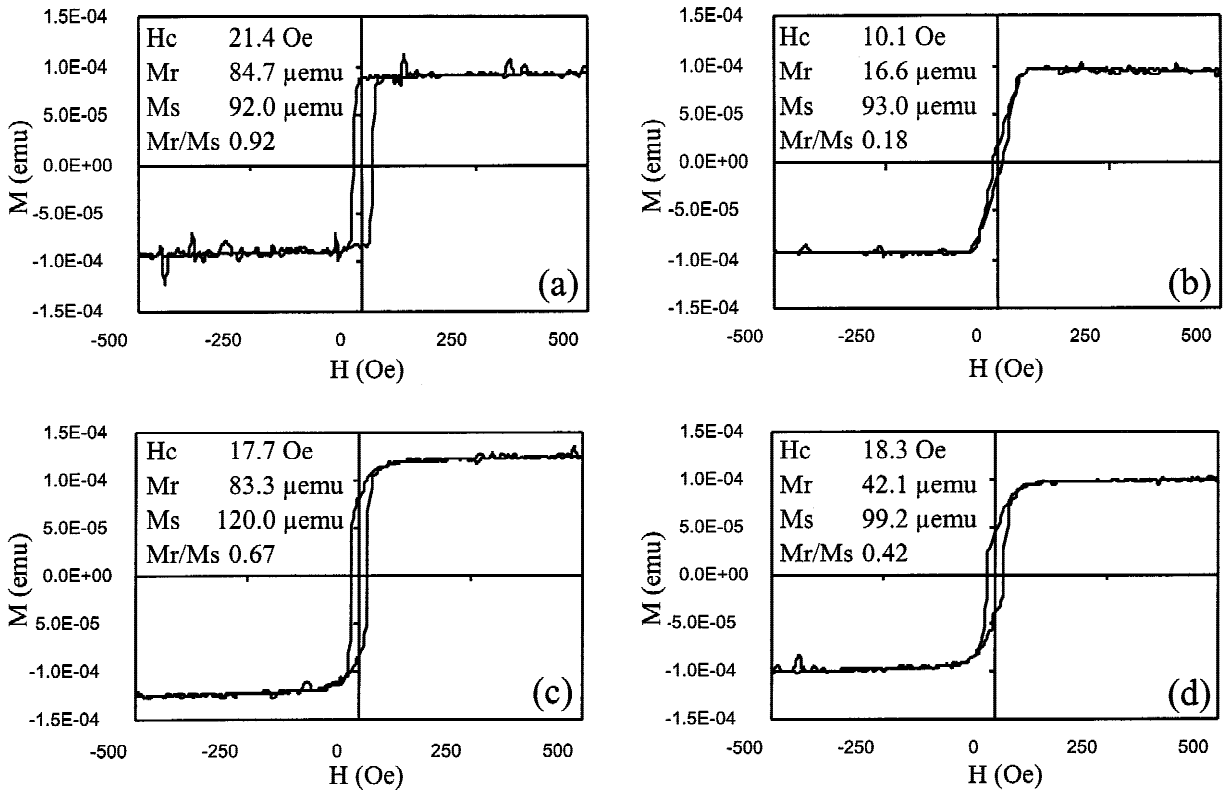


**Figure 1.** Magnetization characteristics of $[Co(4.0\ nm)/Cu(x\ nm)]_4$ multilayers. **a:** $x = 1.5$, **b:** $x = 2.0$, **c:** $x = 2.5$, and **d:** $x = 3.5$.

resistance, $R_0$: resistance in a magnetic free space) to Cu thickness ($t_{Cu}$) curve, where $\Delta R/R_0$ is about one-half the first maximum ($t_{Cu} \sim 0.8$ nm; Dorner et al., 1993). Four kinds of samples, $Si/[Co(4.0\ nm)/Cu(2.0\ nm)]_n$, where $n =$ 4, 5, 6, and $Si/[Co(14.0\ nm)/Cu(2.2\ nm)]_5$, have been investigated by electron holography. Specimens for the cross-sectional observation are prepared in a conventional manner, by mechanical dimpling and ion milling. Angles of ion guns were set so that the specimens had wedges of 20° for $Si/[Co(4.0\ nm)/Cu(2.0\ nm)]_n$ and 10° for $Si/[Co(14.0\ nm)/Cu(2.2\ nm)]_5$.

## Phase-Shifting Electron Holography

Two kinds of electron holography were utilized in the observation of multilayers: a Fourier method and a phase-shifting method.

The Fourier method, which is the most popular method, requires only one hologram to reconstruct a wave function and has a large allowance for localized defects of holograms. However, a filter mask inserted in the Fourier plane to pass only the side band spectrum in reconstructing an object wave intrinsically restricts the spatial resolution that can be attained. The resolution is limited by the radius of the filter mask, and available mask radius is determined by a carrier frequency, that is, the spacing of interference fringes. The resolution is about double the fringe spacing (in a low-resolution image) or three times the fringe spacing (in a high-resolution image) (Tanji et al., 1993; Orchowski et al., 1995). Moreover, the interference width strongly depends on the imaging mode: In our holographic microscope, the width is up to 10 nm with a resolution better than 0.2 nm, and 3 $\mu$m with 30-nm resolution. If we require an interference width of 50 nm, the spatial resolution of a reconstructed image with a high S-N ratio is restricted to 1–1.5 nm, although this width differs from one instrument to another.

The phase-shifting method (Ru et al., 1991) reconstructs the wave function on each pixel from a series of holograms whose interference fringes are shifted one after another. The shifting of the interference fringes, that is, the shift of initial phase difference between an object wave and a reference wave, is carried out by tilting an incident electron wave as shown in Figure 2. When the incident electron wave is tilted to $\theta_n$, the object wave $\Psi_0$ and the reference wave $\Psi_r$ are expressed as

$$\Psi_0(x_0, y_0) = A(x_0, y_0) \times \exp[i\{kz - k\theta_n x_0 - \tfrac{1}{2}k\theta_n w + \phi(x_0, y_0)\}], \quad (1)$$

$$\Psi_r(x_0, y_0) = \exp[i\{kz - k\theta_n x_0 + \tfrac{1}{2}k\theta_n w\}], \quad (2)$$

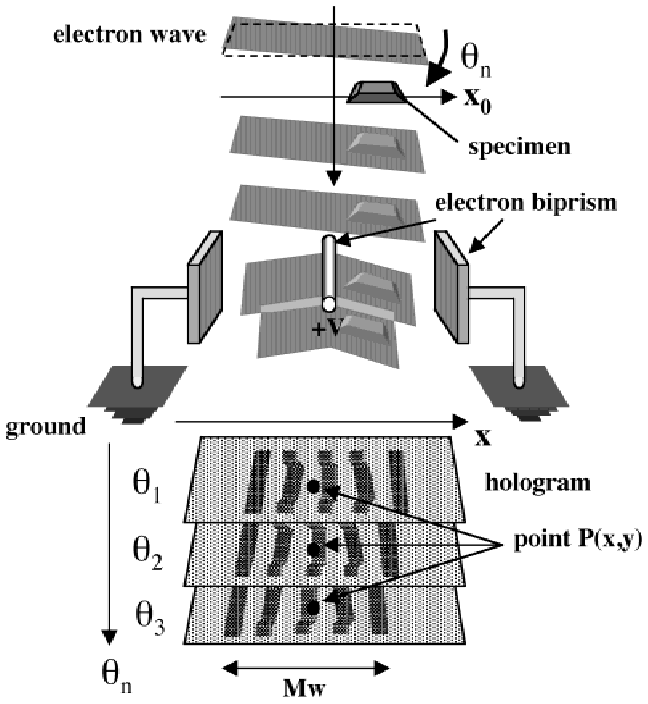


**Figure 2.** Schematic of phase-shifting electron holography. Interference fringes are shifted by tilting an incident electron wave.

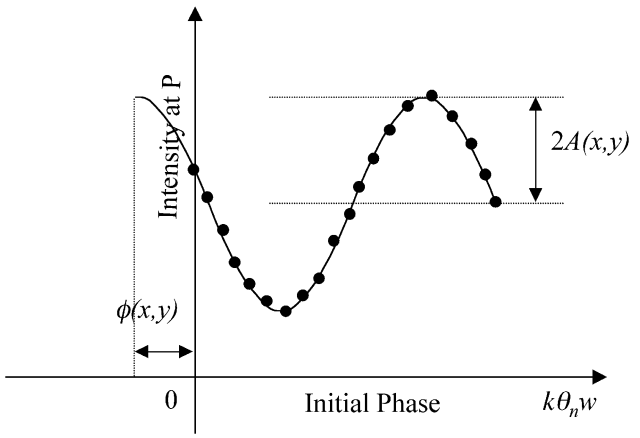


**Figure 3.** Procedure for reconstructing the object wave at point P$(x, y)$. The amplitude $A(x, y)$ and phase $\phi(x, y)$ of the object wave are derived from the intensity variation against the initial phase.

where $x_0$ and $y_0$ are coordinates in an object plane, $A(x_0, y_0)$ and $\phi(x_0, y_0)$ are the amplitude and phase of the object wave, respectively, $w$ is the interference width, $n$ is an integer specifying the hologram, and $k = 2\pi/\lambda$, where $\lambda$ is the wavelength.

Interfering through an electron biprism, two waves $\Psi_0$ and $\Psi_r$ construct a hologram whose intensity is expressed as

$$I(x, y, n) = |\Psi_0 + \Psi_r|^2 = 1 + |A(x, y)|^2 + 2A(x, y)\cos\{2k\alpha x - \phi(x, y) + k\theta_n w\}, \quad (3)$$

where $x$ and $y$ are coordinates in the image plane, $\alpha$ is the angle of the electron waves deflected by the electron biprism, and the magnification is assumed to be unity.

The phase term $k\theta_n w$ is the initial phase difference between the object wave and the reference wave in the $n$th hologram. Therefore, we can shift the interference fringes by tilting the incident electron wave.

The object wave is reconstructed from a series of such holograms. When the interference fringes are shifted, intensities at the same point P$(x, y)$ on each hologram vary sinusoidally. In Figure 3, the intensity at point P is plotted on a diagram as a function of $k\theta_n w$ and fitted to a sinusoidal curve. The phase term $2k\alpha x$ in equation (3) is closely related to the carrier frequency of the interference fringes, and is determined from Fourier transformation of the hologram. Therefore, the amplitude $A(x, y)$ and the phase $\theta(x, y)$ at point P are picked out from the curve. For the other points, the values of the amplitude and phase are determined independently in the same manner, to thereby yield the reconstructed image.

Although the phase-shifting method requires much longer time for recording and reconstruction than does the Fourier method, it yields an advantage that the resolution of reconstructed images depends not on the spacing of the interference fringes, but on the resolving power of the microscope and the pixel size of a CCD converted on the specimen plane, allowing use of high S/N holograms with thicker fringes. In the present experiment, 13 holograms with different initial phases were used in the reconstruction. The phase-shifting method is strongly influenced by the fluctuation of the image position produced by specimen drift, mechanical vibration, and other causes. Therefore, position adjustment of a few pixels plays a very important role for the accuracy of reconstruction. Furthermore, the Fresnel diffraction at the electron biprism greatly influences the reconstruction and must be corrected in order to obtain a high-resolution and high-sensitivity observation. Nonuniform intensity of interference fringes is corrected by an envelope function, by tracing all maxima and minima. Phase deviation due to the Fresnel diffraction is subtracted by use of reference holograms (Yamamoto et al., 2000).

## Prediction of Phase Shift

Before results are analyzed, forecasting the phase shift in the specimen is worthwhile. If the magnetization vectors in all Co layers are directed upward, as indicated with arrowheads toward N poles in Figure 4a, the electron phase proceeds rightward as shown in Figure 4b, whereas the difference of mean inner-potential between Co and Cu produces the phase difference as in Figure 4c, resulting in the observed

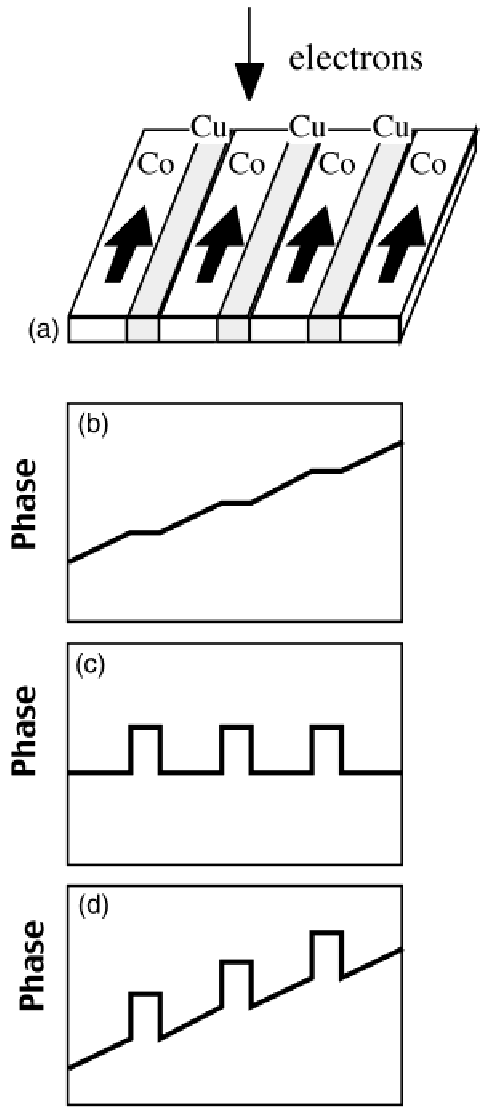


**Figure 4.** Schema of a phase distribution observed by electron holography. In the case where all the magnetization vectors are aligned parallel (**a**), the phase shift due to the magnetization (**b**) and the difference of mean inner-potentials between Co and Cu (**c**) will yield the observed final phase distribution (**d**).

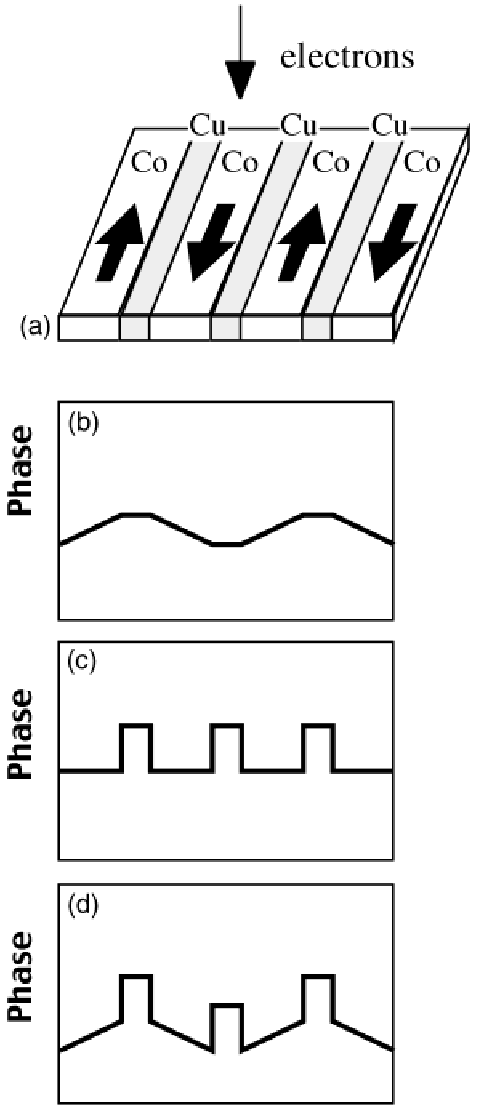


**Figure 5.** Schema of a phase distribution observed by electron holography. In the case where all the magnetization vectors are aligned antiparallel (**a**), the phase shift due to the magnetization (**b**) and the difference of mean inner-potentials between Co and Cu (**c**) will yield the observed final phase distribution (**d**).

phase distribution shown in Figure 4d. On the other hand, if the magnetization aligns antiparallel, as illustrated in Figure 5a, the electron phase changes in a zigzag pattern as shown in Figure 5b, the effect of mean inner-potential remains, and observed phase will be distributed as shown in Figure 5d.

## Results and Discussion

Observation was performed by use of a field emission TEM, Hitachi HF-2000, equipped with an electron biprism, low magnetic field objective lens (Hirayama et al., 1993), and a slow scan CCD camera (Gatan 694).

Figure 6 shows a TEM image of [Co (4.0 nm)/Cu (2.0 nm)]$_5$ (Fig. 6a) and its hologram (Fig. 6b). The TEM image was obtained in slight underfocus and the hologram was recorded after refocusing. In this hologram, the spacing of interference fringes is about 0.8 nm with an interference width of 40 nm, and in other cases, the spacing was 0.6–0.8 nm. To distinguish the layers from Fresnel fringes in reconstructed images, holograms were taken so that interference fringes inclined about 2° toward the stacking layers. Figure 7 shows a TEM image of [Co(4.0 nm)/Cu(2.0 nm)]$_6$ (Fig. 7a), a phase image reconstructed by the Fourier method

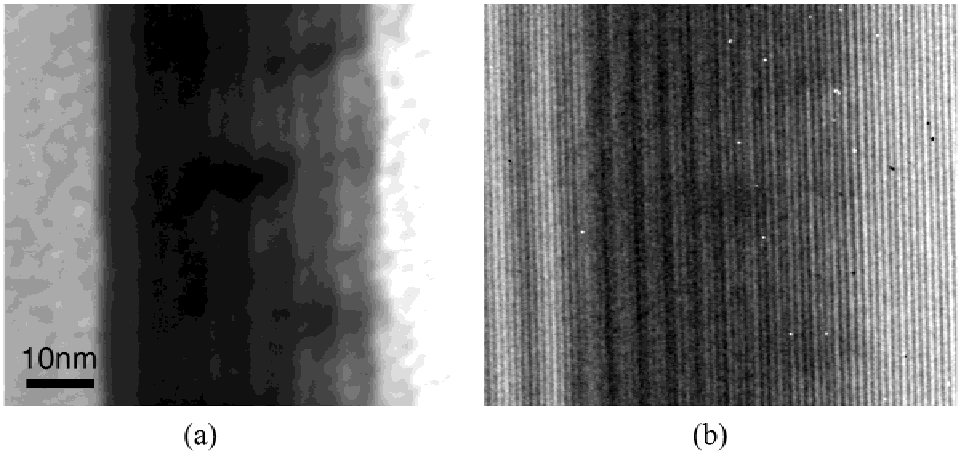


**Figure 6.** TEM image of $[Co(4.0\ nm)/Cu(2.0\ nm)]_6$ (**a**) and an electron hologram (**b**). The TEM image was taken in slight underfocus and the hologram was recorded after refocusing.

(Fig. 7b), and line-profiles of the two images (Fig. 7c,d). In the phase image, the influence of inner-potential difference due to the wedge shape has been subtracted, by assuming the angle of the wedge to be 20° or 10° as described in the section titled Specimen, and estimating mean inner potentials as $V_{Co} = 29.6$ eV and $V_{Cu} = 22.7$ eV with forward atomic scattering factors $f_{Cu}(0)$ and $f_{Co}(0)$ (Doyle & Turner, 1968; Dunin-Borkowski, 2000). Strictly speaking, the influence of the wedge shape on the magnetic phase shift remains, but it does not affect the determination of magnetizing direction. The influence of the wedge shape must be taken into consideration in the quantitative analysis of magnetization. Line profiles were averaged over the region about 1.5 nm along the layers. Comparing with Figure 4, we find that magnetization vectors in all the Co layers clearly align in parallel as indicated with arrowheads (Fig. 7e). Figure 8 shows the observation of $[Co(4.0\ nm)/Cu(2.0\ nm)]_5$. In this specimen, magnetization vectors are separated into two groups, that is, downward in the left two layers and upward in the right three layers as shown in Figure 8e. The difference between the two magnetic structures in Figures 7 and 8 seems not to be substantial, but to be caused by the small fluctuation of $t_{Cu}$ or too small number of layers.

Because the spatial resolution of images reconstructed is poorer than 1.5 nm, boundary regions between Co and Cu layers are unreliable in these figures. The phase-shifting method has a capability to resolve up to the pixel size, although a small averaging ($3 \times 3$) was applied to raw reconstructed images. Figure 9 shows the images of $[Co(14.0\ nm)/Cu(2.2\ nm)]_5$. The TEM image (Fig. 9a) shows that the widths of Cu and Co layers coincide with expected values. Figure 9b shows a reconstructed phase image obtained by the phase-shifting method. Its line profile is shown in Figure 9c. As before, the influence of the 10° wedge shape has been removed. The line profile was averaged over the region of 1 nm along the layers. The quality is

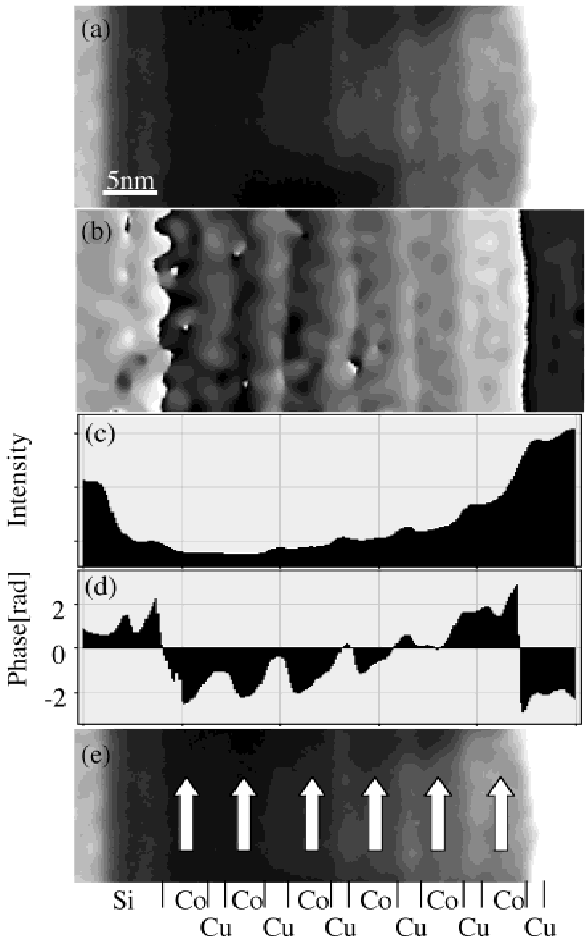


**Figure 7.** Electron holography of $[Co(4.0\ nm)/Cu(2.0\ nm)]_6$ obtained by the Fourier method. The intensity of a TEM image (**a**) and the phase angle of a reconstructed phase image (**b**) are profiled with averaging 20 pixels along the layers (**c**, **d**). The profiled phase shows that all the Co layers have magnetic vectors aligned parallel (**e**). The interference region is about 50 nm.

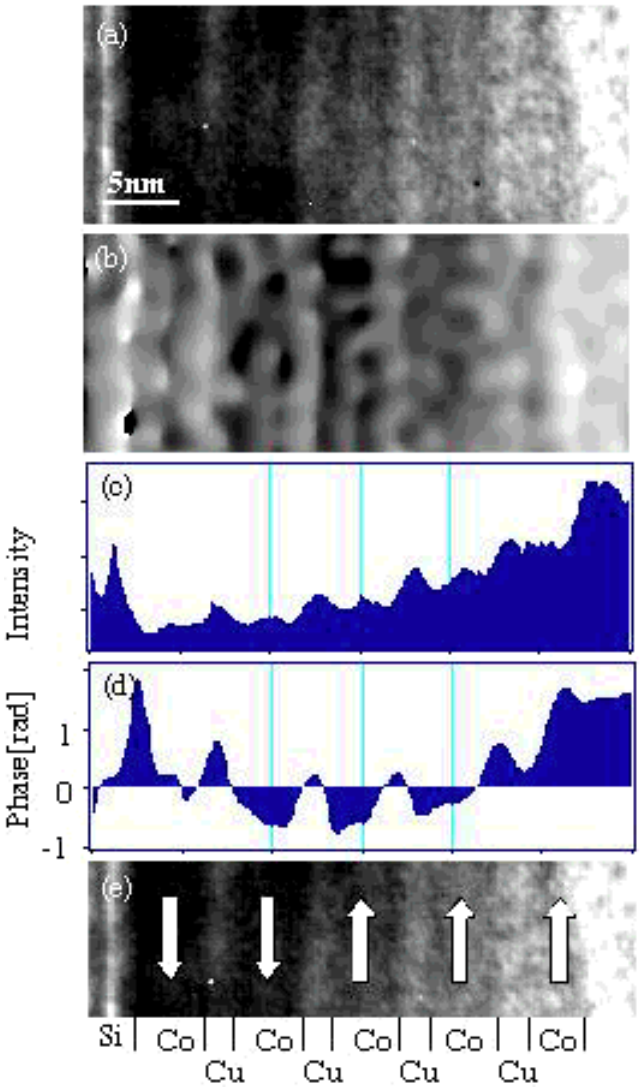


**Figure 8.** Electron holography of $[Co(4.0\ nm)/Cu(2.0\ nm)]_5$ obtained by the Fourier method. The intensity of a TEM image (**a**) and the phase angle of a reconstructed phase image (**b**) are profiled with averaging 20 pixels along the layers (**c**, **d**). The profiled phase shows that the Co layers form two groups, of two and three, in which magnetic vectors are aligned parallel (**e**). The interference region is about 40 nm.

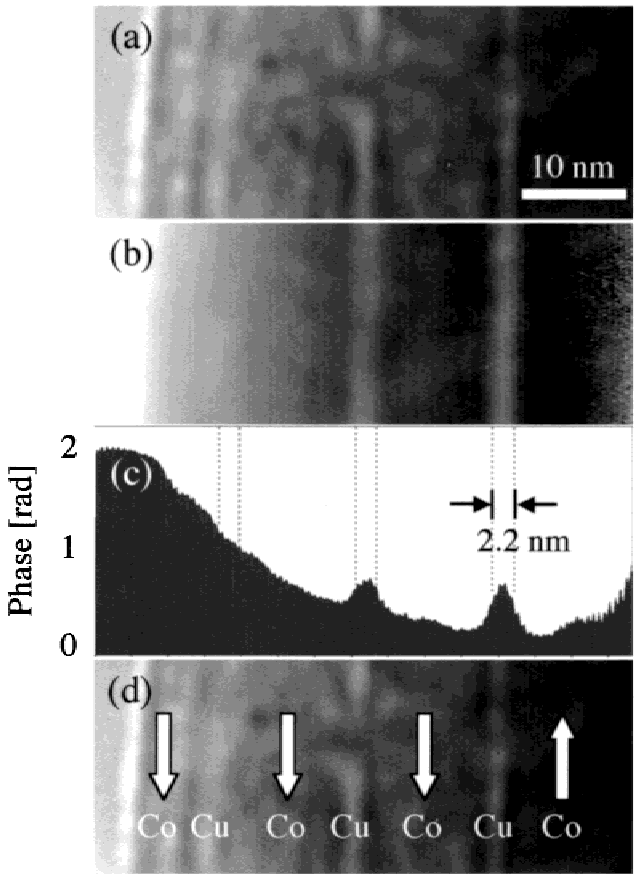


**Figure 9.** Phase-shifting electron holography of $[Co(12.0\ nm)/Cu(2.2\ nm)]_5$. Only four layers of Co/Cu appear in a TEM image (**a**). A reconstructed phase image (**b**) and its line profile (**c**) show the direction of magnetic vectors in (**d**). The interference region is about 60 nm.

distinctly higher than that obtained by the Fourier method. Because the interference width is less than 60 nm under this electrooptical condition, only four Co layers are observed in the reconstructed image. As indicated in Figure 9d, in the left three layers magnetization vectors are aligned downward, and in the right-end layer the magnetization vector is oriented upward. About 25% of the investigated samples of $t_{Cu} = 2.0$ nm and 80% of samples $t_{Cu} = 2.2$ nm show the same structure, in which two blocks with antiparallel magnetization vectors are separated, and the other samples show the parallel alignment of magnetization vectors. If specimens consisted of a larger number of layers, they might show more blocks with antiparallel alignment. Thus far, the alignment in which each vector is antiparallel to the adjacent ferromagnetic layers has not been obtained. This seems to be the reason why the magnetization characteristic in Figure 1b does not show exact antiferromagnetism, but weak ferromagnetism with finite residual magnetization (Mr) and coercive force (Hc), and magnetoresistance ratio $\Delta R/R_0$ ($\Delta R$: decrease of resistance, $R_0$: resistance in a magnetic free space) is about a half the first maximum. The spatial resolution is about 0.3 nm in principle, which allows us to discuss the magnetic structure at the boundaries. Figure 9c reveals that the regions of 1–1.5 nm width at the boundaries are distorted, that is, the magnetization in the region of 1–1.5 nm inside the Co layer is weakened and that of ~0.5 nm inside the Cu layer is magnetized slightly. Although some atomic roughness may be present at boundaries and not distinguishable in the TEM image in Figure 9a, the magnetic mixture of 1–1.5 nm width seems to be wider than that reported previously (Zweck et al., 1997; Marrows et al., 2000).

## Conclusion

Electron holography was applied to the observation of magnetic fine structures of Co/Cu multilayers. Cross-sectional observation was performed for four kinds of samples with different numbers of layers and with Co layers of different thicknesses. The advantage of the phase-shifting method over the Fourier method in the observation of magnetic multilayers was demonstrated. Reconstructed phase images clearly showed the alignment of magnetization vectors in Co layers, some of which were separated into two blocks with antiparallel alignment. Meanwhile, no specimen has shown the alignment in which all the vectors are antiparallel to adjacent ferromagnetic layers. This seems to be the reason why the magnetoresistance ratio of the specimen with Cu spacers 2–2.2 nm thick is on the second maximum of $\Delta R/R_0$, which is half the first maximum. The magnetic mixture on interfaces is 1.0–1.5 nm, which seems to be wider than atomic roughness.

Finally, we note that the phase-shifting method has an advantage of high spatial resolution and high sensitivity, but simultaneously has disadvantages that, in principle, a longer time is required for acquiring a series of holograms and processing them, and, in practice, each hologram must be aligned with the same accuracy as the desired spatial resolution, when images of specimen drift for some reason.

## References

Baibich, M.N., Broto, J.M., Fert, A., Nguyen Van Dau, F., Petroff, F., Etienne, P., Creuzet, G., Friederich, A. & Chazelas, J. (1988). Giant magnetoresistance of (001)Fe/(001)Cr magnetic superlattices. *Phys Rev Lett* **61**, 2472–2475.

Dorner, C., Haidl, M. & Hoffmann, H. (1993). Giant magnetoresistance of Co/Cu multilayers with and without Fe buffer layers. *J Appl Phys* **74**, 5886–5888.

Doyle, P.A. & Turner, P.S. (1968). Relativistic Hartree-Fock x-ray and electron scattering factors. *Acta Cryst A* **24**, 390–397.

Dunin-Borkowski, R.E. (2000). The development of Fresnel contrast analysis, and the interpretation of mean inner potential profiles at interfaces. *Ultramicroscopy* **83**, 193–216.

Hirayama, T., Ru, Q., Tanji, T. & Tonomura, A. (1993). Observation of magnetic-domain states of barium ferrite particles by electron holography. *Appl Phys Lett* **63**, 418–420.

Marrows, C.H., Hickey, B.J., Herrmann, M., McVitie, S., Chapman, J.N., Ormston, M., Petford-Long, A.K., Hase, T.P.A. & Tanner, B.K. (2000). Damage caused to interlayer coupling of magnetic multilayers by residual gases. *Phys Rev* **61**, 4131–4140.

Orchowski, A., Rau, W.D. & Lichte, H. (1995). Electron holography surmounts resolution limit of electron microscopy. *Phys Rev Lett* **74**, 399–402.

Parkin, S.S.P., More, N. & Roche, K. (1990). Oscillations in exchange coupling and magnetoresistance in metallic superlattice structures: Co/Ru, Co/Cr, and Fe/Cr. *Phys Rev Lett* **64**, 2304–2307.

Ru, Q., Endo, J., Tanji, T. & Tonomura, A. (1991). Phase-shifting electron holography by beam tilting. *Appl Phys Lett* **59**, 2372–2374.

Tanji, T., Hasebe, S. & Suzuki, T. (2002). Holographic observation of magnetic fine-structures in new magnetic materials. *Microsc Microanal* **8**(Suppl. 2), 30–31.

Tanji, T., Urata, K., Ishizuka, K., Ru, Q. & Tonomura, A. (1993). Observation of atomic surface potential by electron holography. *Ultramicroscopy* **49**, 259–264.

Yamamoto, K., Kawajiri, I., Tanji, T., Hibino, M. & Hirayama, T. (2000). High precision phase-shifting electron holography. *J Electron Microsc* **49**, 31–39.

Zweck, J., Zimmermann, T. & Schuhrke, T. (1997). TEM observation and evaluation of magnetic structures in Co/Cu multilayers. *Ultramicroscopy* **67**, 153–162.